Conductance of a Molecular Junction
M. A. Reed, *et al.*
Science **278**, 252 (1997);
DOI: 10.1126/science.278.5336.252

Conductance of a Molecular Junction

M. A. Reed,* C. Zhou, C. J. Muller, T. P. Burgin, J. M. Tour*

Molecules of benzene-1,4-dithiol were self-assembled onto the two facing gold electrodes of a mechanically controllable break junction to form a statically stable gold-sulfur-aryl-sulfur-gold system, allowing for direct observation of charge transport through the molecules. Current-voltage measurements at room temperature demonstrated a highly reproducible apparent gap at about 0.7 volt, and the conductance-voltage curve showed two steps in both bias directions. This study provides a quantative measure of the conductance of a junction containing a single molecule, which is a fundamental step in the emerging area of molecular-scale electronics.

The measurement of charge transport in single organic molecules and the determination of their conductance are long-sought goals. Such measurements are experimentally challenging and intriguing because one can test the validity of transport approximations at the molecular level. A conceptually simple configuration would be to connect a single molecule between metallic contacts. Such a metal-molecule-metal configuration would present the molecular embodiment of a system analogous to a quantum dot (*1*–*9*), with the potential barriers of the semiconductor system being replaced by any existing contact barrier of the molecule-metal interface.

Previous measurements on atomic and molecular systems have been made with scanning tunneling microscopes (STMs) (*10*–*12*) and can yield conductivity information (*13*–*15*). Experiments with an evaporated-metal-top-contact/molecules/metallic-bottom-contact configuration, which has ten of thousands of parallel active molecules, have also been demonstrated (*16*, *17*). One experiment on an organic system (*18*) reported evidence for Coulomb charging.

We have performed measurements in the configuration of a single molecule between metallic contacts; specifically, on benzene-1,4-dithiolate connected between stable, proximal, metallic gold contacts at room temperature. This approach complements previous approaches by presenting statically stable contacts and concurrently restricts the number of active molecules to as few as one.

Experiments were conducted at room temperature with a mechanically controllable break junction (MCB) (*19*) (Fig. 1). In this approach, a notched metal wire is glued onto a flexible substrate and is fractured by bending of the substrate, after which an adjustable tunneling gap can be established. A large reduction factor between the piezo elongation and the electrode separation ensures an inherently stable contact or tunnel junction. The wire contacts are atomically sharp when broken, which is demonstrated in the conductance quantization as previously reported (*20*). In the experiments reported here, benzene-1,4-dithiol was adsorbed from a 1 mM solution in tetrahydrofuran (THF) onto the two facing gold electrodes of the break junction, which were broken in solution under an Ar atmosphere (*21*), resulting in formation of a self-assembled monolayer (SAM) on the gold electrodes that was nearly perpendicular to the surface (*21*). The THF solvent was allowed to evaporate in the ambient Ar atmosphere before the conductance measurements, and there was no further surface preparation or cleaning. The removal of the THF led to thermal gradients that disturbed the picometer static dimensional stability of the MCB, requiring the tips to be withdrawn and then returned to measure the electrical properties of the molecule or molecules adsorbed on the surfaces (Fig. 2). The configuration shown in Fig. 3 is probable because the displacement of thiols has been shown (*10*) and the formation of a disulfide bridge would require oxygen (*21*).

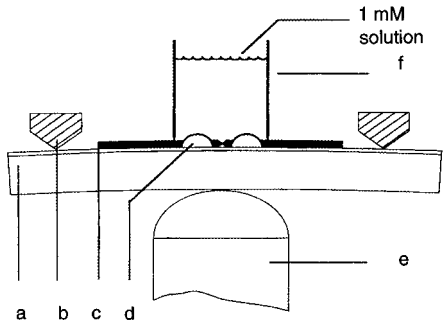

Fig. 1. A schematic of the MCB junction with (a) the bending beam, (b) the counter supports, (c) the notched gold wire, (d) the glue contacts, (e) the pizeo element, and (f) the glass tube containing the solution.

As the tips were brought together, current-voltage $I(V)$ and conductance $G(V)$ $(= dI/dV)$ measurements showed characteristic features (Fig. 4A) that proved to be highly reproducible (Fig. 4B). The spacing between the electrodes was ~8 Å, set by the pizeo voltage as determined by previous calibration of the spacing–to–pizeo voltage conversion factor established by the expotential dependence of the current with distance in the tunneling regime (*22*). However, calibration shift due to solvent evaporation cannot be eliminated. By comparison, an approximate molecule length of 8.46 Å was calculated with the use of an MM2 force field and by measuring to the

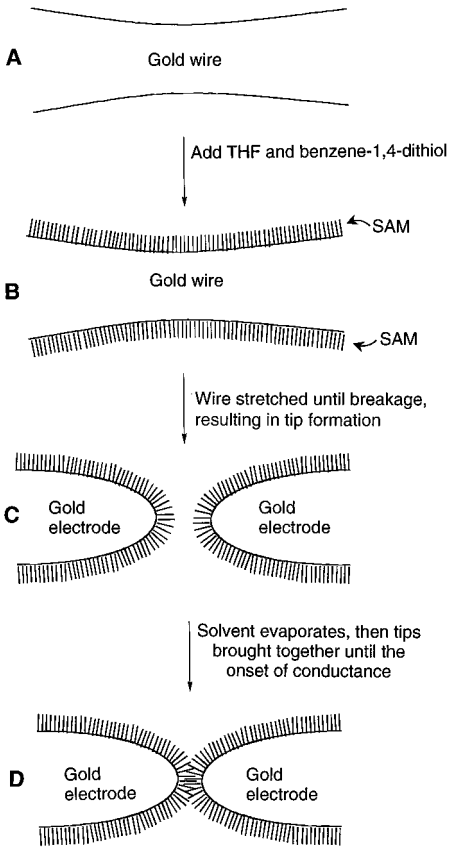

Fig. 2. Schematic of the measurement process. (**A**) The gold wire of the break junction before breaking and tip formation. (**B**) After addition of benzene-1,4-dithiol, SAMs form on the gold wire surfaces. (**C**) Mechanical breakage of the wire in solution produces two opposing gold contacts that are SAM-covered. (**D**) After the solvent is evaporated, the gold contacts are slowly moved together until the onset of conductance is achieved. Steps (C) and (D) (without solution) can be repeated numerous times to test for reprodicibility.

M. A. Reed, C. Zhou, C. J. Muller, Department of Electrical Engineering, Yale University, Post Office Box 208284, New Haven, CT 06520, USA.
T. P. Burgin and J. M. Tour, Department of Chemistry and Biochemistry, University of South Carolina, Columbia, SC 29208, USA.
*To whom correspondence should be addressed.

center of the two gold radii minus the covalent radii of both gold atoms. An apparent gap of ~0.7 V was observed in all cases. The first derivative of $I(V)$ shows two steps in both bias directions with the lower step ~22.2 megohm (0.045 μS) and the higher step ~13.3 megohm (0.075 μS), possibly indicative of a Coulomb staircase. It is noted that the high Fermi energy of the gold contacts (~2 eV) as compared with the low energies of semiconductor quantum dot systems (<100 meV) precludes the observation of negative differential resistance in the present system (*23*), which is often seen in semiconductor systems (*1–7*). A control experiment with unevaporated THF solvent alone (that is, without the benzene-1,4-dithiolate) exhibited a resistance of 1 to 2 gigohm (linear up to 10 V) independent of electrode spacing, implying ionic conduction through the solvent. When the solvent was evaporated, regular vacuum tunneling with a much higher resistance was observed (*19*), with expotential dependence of the current with applied voltage implying the absence of deleterious effects on the MCB due to the solvent.

The first step for these three measurements gives resistance values of 22.2, 22.2, and 22.7 megohm (top to bottom); the next step gives resistance values of 12.5, 13.3, and 14.3 megohm. This is compared to a resistance of ~9 megohm (*11*) and 18 ± 12 megohm (*12*) deduced from measurements of an ensemble of similar molecules contacted to a gold nanocrystal, and a calculated resistance of this system of 100 kilohm (*24*). A resistance greater than ~22 megohm was not observed in our measurements; however, resistances less than this maximum were occasionally observed. Figure 4C shows $I(V)$ and $G(V)$ measurements of one singular observation that gave resistances that were approximately half (that is, 0.5) the value of the maximum resistances (using averages, 0.63, and 0.45, respectively). This suggests a configuration of two noninteracting self-assembled molecules in parallel, substantiating the idea that the threshold resistance of a single molecule is ~22 megohm, and compares with the previously deduced value of 18 ± 12 megohm of a similar system.

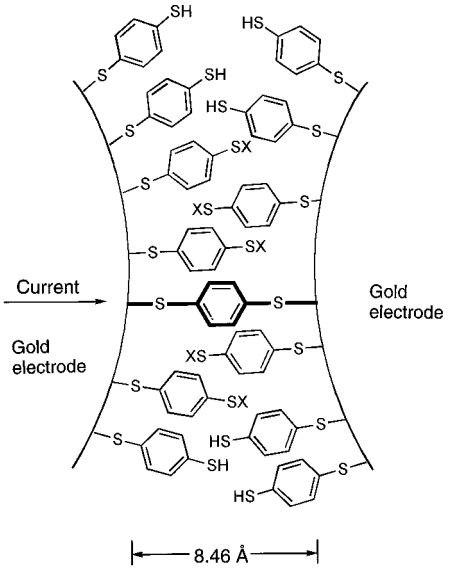

Fig. 3. A schematic of a benzene-1,4-dithiolate SAM between proximal gold electrodes formed in an MCB. The thiolate is normally H-terminated after deposition; end groups denoted as X can be either H or Au, with the Au potentially arising from a previous contact/retraction event. These molecules remain nearly perpendicular to the Au surface, making other molecular orientations unlikely (*21*).

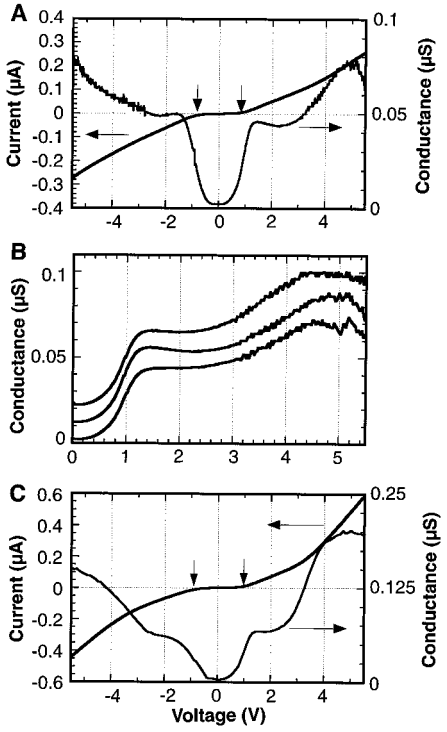

Fig. 4. (**A**) Typical $I(V)$ characteristics, which illustrate a gap of 0.7 V; and the first derivative $G(V)$, which shows a steplike structure. (**B**) Three independent $G(V)$ measurements, offset for clarity, illustrating the reproducibility of the conductance values. The measurements were made with the same MCB but for different retractions/contacts and thus different contact configurations. Offsets of 0.01 μS for the middle curve and 0.02 μS for the top curve are used for clarity. The first step for these three measurements gives values of 22.2, 22.2, and 22.7 megohm (top to bottom); the next step gives values of 12.5, 13.3, and 14.3 megohm. The middle curve is the same data as in (A). (**C**) An $I(V)$ and $G(V)$ measurement illustrating conductance values approximately twice the observed minimum conductance values. Resistances of ~14 megohm for the first step and 7.1 megohm (negative bias) and 5 megohm (positive bias) for the second step were measured.

One interpretation of the observed gap around zero voltage is that it is a Coulomb gap. Using the "apparent" Coulomb gap, an experimental capacitance of 1.1×10^{-19} F is obtained. Although the charge transport through the molecule is in principle a many-body effect, as a first step one can estimate the capacitance of the aryl group with a crude model: A 4.5 Å metallic sphere bound 2.0 Å from proximal metallic planes with intervening vacuum barriers gives a capacitance of 0.4×10^{-19} F, as compared with the experimentally derived 1.1×10^{-19} F. However, a definitive demonstration of Coulomb blockade would require a third gate electrode, which is problematic in the present configuration because a third proximal probe cannot be placed near the molecule. A second interpretation of the observed gap is that it is due to the mismatch between the contact Fermi level and the lowest unoccupied molecular orbital (LUMO). Preliminary calculations using this interpretation give characteristics similar to those of the experimentally observed data (*25*).

The reproducibility of the minimum conductance at a consistent value implies that the number of active molecules could be as few as one. A better theoretical understanding of the threshold resistance of this system, either the apparent Coulomb gap derived from the capacitance of a single molecule configuration or the determination of the contact Fermi level–LUMO gap alignment, is needed to compare to the experimental values of ~22 megohm and ~0.7 V, respectively.

REFERENCES AND NOTES

1. M. A. Reed *et al.*, *Phys. Rev. Lett.* **60**, 535 (1988).
2. U. Meirav, M. Kastner, S. Wind, *ibid.* **65**, 771 (1990).
3. M. Dellow *et al.*, *Electron Lett.* **27**, 134 (1991).
4. L. P. Kouwenhoven *et al.*, *Z. Phys. B* **85**, 367 (1991); L. P. Kouwenhoven *et al.*, *ibid.*, p. 381.
5. M. Tewordt *et al.*, *Phys. Rev. B* **46**, 3948 (1992).
6. B. Su, V. Goldman, J. Cunningham, *ibid.*, p. 7644.
7. D. L. Klein, P. L. McEuen, J. E. B. Katari, R. Roth, A. P. Alivisatos, *Appl. Phys. Lett.* **68**, 2574 (1996).
8. C. T. Black, D. C. Ralph, M. Tinkham, *Phys. Rev. Lett.* **76**, 688 (1996).
9. H. Grabert, J. M. Martinis, M. H. Devoret, Eds., *Single Charge Tunneling* (Plenum, New York, 1991).
10. L. A. Bumm *et al.*, *Science* **271**, 1705 (1996).
11. M. Dorogi, J. Gomez, R. Osifchin, R. P. Andres, R. Reifenberger, *Phys. Rev. B* **52**, 9071 (1995).
12. R. P. Andres *et al.*, *Science* **272**, 1323 (1996).
13. M. F. Crommie, C. P. Lutz, D. M. Eigler, *Phys. Rev.* **B48**, 2851 (1993).
14. C. Joachim, J. K. Gimzewski, R. R. Schlittler, C. Chavy, *Phys. Rev. Lett.* **74**, 2102 (1995); C. Joachim and J. K. Gimzewski, *Europhys. Lett.* **30**, 409 (1995).
15. A. Yazdani, D. M. Eigler, N. D. Lang, *Science* **272**, 1921 (1996); A. Yazdani, B. A. Jones, C. P. Lutz, M. F. Crommie, D. M. Eigler, *ibid.* **275**, 1767 (1997).
16. C. M. Fischer, M. Burghard, S. Roth, K v. Klitzing, *Appl. Phys. Lett.* **66**, 3331 (1995).
17. H. Grabert, *Z. Phys. B* **85**, 319 (1991).
18. H. Nejoh, *Nature* **353**, 640 (1991).
19. C. J. Muller, J. M. van Ruitenbeek, L. J. de Jongh,

Physica C **191**, 485 (1992).
20. C. J. Muller *et al.*, *Phys. Rev. B* **53**, 1022 (1996), and references therein.
21. J. M. Tour *et al.*, *J. Am. Chem. Soc.* **117**, 9529 (1995).
22. C. Zhou, C. J. Muller, M. R. Deshpande, J. W. Sleight, M. A. Reed, *Appl. Phys. Lett.* **67**, 1160 (1995).
23. V. Mujica, M. Kemp, A. Roitberg, M. Ratner, *J. Chem. Phys.* **104**, 7296 (1996).
24. M. P. Samanta *et al.*, *Phys. Rev.* **53B**, R7626 (1996).
25. S. Datta *et al.*, *Phys. Rev. Lett.*, in press; W. Tian *et al.*, *Physica E*, in press.
26. We thank M. R. Deshpande for fruitful discussions and the Defense Advanced Research Projects Agency for support.

25 April 1997; accepted 22 August 1997

Depth Extent of the Lau Back-Arc Spreading Center and Its Relation to Subduction Processes

Dapeng Zhao,* Yingbiao Xu, Douglas A. Wiens, LeRoy Dorman, John Hildebrand, Spahr Webb

Seismic tomography and wave form inversion revealed that very slow velocity anomalies (5 to 7 percent) beneath the active Lau spreading center extend to 100-kilometer depth and are connected to moderately slow anomalies (2 to 4 percent) in the mantle wedge to 400-kilometer depth. These results indicate that geodynamic systems associated with back-arc spreading are related to deep processes, such as the convective circulation in the mantle wedge and deep dehydration reactions in the subducting slab. The slow regions associated with the Tonga arc and the Lau back arc are separated at shallow levels but merge at depths greater than 100 kilometers, suggesting that slab components of back-arc magmas occur through mixing at these depths.

Knowledge of the seismic structure beneath back-arc spreading centers is important because the width and depth of the slow-velocity regions below spreading centers provide constraints on the origin of back-arc spreading (*1*, *2*), the geochemical source of arc and back-arc magmas (*3*), the interaction between subduction and back-arc spreading (*1*), whether the mantle upwelling beneath spreading centers is passive or active, and to what depth the upwelling persists (*2*). A subduction zone with an associated back-arc spreading center and the existence of deep earthquakes immediately beneath the center provide an ideal geometry to image and understand back-arc spreading processes. The Tonga-Fiji region, which contains two-thirds of all deep earthquakes in the world, represents an optimal region for exploring these questions. Previous studies have discussed the seismic velocity anomalies due to the Tonga slab (*4*, *5*), but this work has been hampered by the poor distribution of seismic stations.

The installation (*6*) of 12 broadband stations in the Tonga and Fiji islands from November 1993 through December 1995 and a related 3-month deployment of 25 ocean bottom seismometers (OBS) (*7*) in the Lau back arc and the Tonga forearc provided a unique opportunity to determine high-resolution three-dimensional (3D) structure in this region (Fig. 1A). We used 41,471 arrival times from 926 earthquakes that occurred in the Tonga-Fiji region during the seismic experiment (Fig. 1B). Most of the events were associated with the subduction of the Tonga slab; they had a relatively uniform distribution in the entire upper mantle. This uniform distribution is an advantageous feature over other subduction zones, such as Japan and Alaska, where most of the seismicity is concentrated at depths shallower than 250 km (*8*, *9*). We picked about 8200 arrival times at the 12 land stations from the 926 earthquakes and about 2900 arrivals at the 25 OBS stations from 250 earthquakes that occurred during the OBS deployment. The picking accuracy is estimated to be 0.05 to 0.3 s. The remaining arrival times were recorded by stations reporting to the Preliminary Determination of Epicenters (PDE) with epicentral distances up to 90°. The PDE arrival times have lower quality (picking accuracy of 0.2 to 0.5 s), so they were assigned less than half the weight of the local data. All of the 926 earthquakes were recorded by more than 20 stations, and their hypocentral locations have a statistical accuracy of ±3 to 9 km. We also picked 450 arrival times at the 12 land and 25 OBS stations from 45 large (magnitude of 6.0 to 8.0) teleseismic events with epicentral distances from 30° to 90°, which were assigned the same weight as the local data in the inversion.

We used a tomography method (*9*) to determine the 3D *P* wave velocity structure in the Tonga-Fiji region (*9*, *10*) (Figs. 2 and 3). To confirm that the major velocity features were adequately resolved by the inversion, we conducted checkerboard resolution tests (*11*) (Fig. 4). The checkerboard test with a grid spacing of 50 km indicates good resolution for the area in and around the subducting Tonga slab and along the main line of OBSs (Fig. 4, A and B). For the test with a grid spacing of 70 km, the resolution is good for all the areas discussed (Fig. 4, C and D). We also conducted a number of inversions and resolution tests by changing the grid spacing, the grid configuration, and the initial model (*10*). The results show that the velocity structure in the study area (Fig. 3) can be resolved with a resolution of 50 to 70 km. This resolution scale is better than the 100- to 200-km resolution ob-

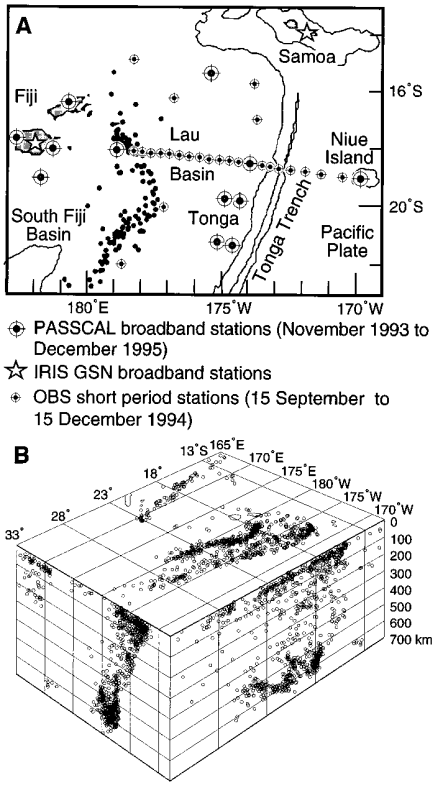

Fig. 1. (**A**) Map showing the seismometer deployments in the Fiji-Tonga region. Twelve broadband instrument island sites, 25 OBS sites, and two PDE sites (at Samoa and Fiji) recorded the data used in this study. A 2-year sample of deep earthquakes (depths of 300 to 680 km and $m_b > 4.8$) (dots) delineates the deep Tonga slab. PASSCAL, Program for Array Seismic Studies of the Continental Lithosphere; IRIS, Incorporated Research Institutions in Seismology; GSN, Global Seismographic Network. (**B**) Hypocentral distribution of the 926 earthquakes used in this study.

D. Zhao, Southern California Earthquake Center and Department of Earth Sciences, University of Southern California, Los Angeles, CA 90089, USA.
Y. Xu and D. A. Wiens, Department of Earth and Planetary Sciences, Washington University, St. Louis, MO 63130, USA.
L. Dorman, J. Hildebrand, S. Webb, Scripps Institution of Oceanography, University of California, San Diego, La Jolla, CA 92093, USA.

*To whom correspondence should be addressed. E-mail: dzhao@usc.edu